TWO-DIMENSIONAL MATHEMATICAL MODEL OF LIQUID FUEL COMBUSTION IN BUBBLING FLUIDIZED BED APPLIED FOR A FLUIDIZED FURNACE NUMERICAL SIMULATION

by

Stevan Dj. NEMODA*, Milijana J. PAPRIKA, Milica R. MLADENOVIĆ, Ana D. MARINKOVIĆ, and Goran S. ŽIVKOVIĆ

Laboratory for Thermal Engineering and Energy, Vinca Institute of Nuclear Sciences, University of Belgrade, Belgrade, Serbia

Original scientific paper
https://doi.org/10.2298/TSCI170922307N

Lately, experimental methods and numerical simulations are equally employed for the purpose of developing incineration bubbling fluidized bed (BFB) facilities. The paper presents the results of the 2-D CFD model of liquid fuel combustion in BFB, applied for numerical simulation of a fluidized bed furnace. The numerical procedure is based on the two-fluid Euler-Euler approach, where the velocity field of the gas and particles are modeled in analogy to the kinetic gas theory. The proposed numerical model comprises energy equations for all three phases (gas, inert fluidized particles, and liquid fuel), as well as the transport equations of chemical components that are participating in the reactions of combustion and devolatilization. The model equations are solved applying a commercial CFD package, whereby the user submodels were developed for heterogenic fluidized bed combustion of liquid fuels and for interphase drag forces for all three phases. The results of temperature field calculation were compared with the experiments, carried out in-house, on a BFB pilot facility. The numerical experiments, based on the proposed mathematical model, have been used for the purposes of analyzing the impacts of various fuel flow rates, and fluidization numbers, on the combustion efficiency and on the temperature fields in the combustion zone.

Key words: *CFD model, combustion, liquid fuel, bubbling fluidized bed, Euler-Euler approach, three phase flow*

Introduction

Fluidized bed (FB) incineration, *i. e.* combustion and co-combustion, is a very efficient technology for removing the redundant industrial byproducts. In the case that the combustion of the waste substances has positive energy effects, the FB technology has a great importance not only in terms of preserving the environment but also for the purpose of energy efficiency and utilization of renewable energy sources.

Benefits of combusting unconventional fuels in a BFB are numerous. The unconventional fuels are substances that can be combusted in conventional furnaces, but with great difficulty, due to its high viscosities, low heating value, and content of ballast substances (water and other incombustible materials). Advantages of the FB combustion are primarily the high heat capacity and thermal conductivity of the bed, and intense heat transfer between particles

* Corresponding author, e-mail: snemoda@vinca.rs

of inert bed material and the fuel, which enables a stable combustion process of a wide range of the unconventional fuels, with very low sensitivity to changes in fuel quality. The zone of intense combustion in a FB furnace occupies a relatively small volume because most of the fuel is burned within the bed, with post-combustion of a small portion of the fuel in the *splash* zone and above the bed. In addition, the FB facility may operate at lower temperatures (≈850 °C) which are optimal from the aspect of the reduced concentration of NO_x compounds in the flue gasses. Also, these furnaces are favorable from the aspect of the efficiency of desulfurization by limestone in the furnace [1], when it is necessary.

Lately, experimental methods and numerical simulations are equally employed for the purpose of developing incineration BFB facilities. The CFD models provide great opportunities for saving resources and time in the development of facilities and technologies in the fields of energy and process engineering. However, the numerical tools for simulation of complex processes such as BFB combustion – where it is necessary to simulate complex fluidized granular two-phase flow, including the third-phase of a liquid or solid fuel and homogeneous/heterogeneous chemical reactions – are not completely developed. In addition, it is preferred that the numerical tool is also suitable to engineering needs, meaning it should not require large computational resources and long time.

Two approaches are frequently used for CFD modeling of gas-solid FB: the Euler-Lagrange (EL) approach and the Euler-Euler (EE) approach. In the EL approach [2, 3], the gas-phase is treated as a continuous phase and modeled using a Eulerian framework, whereas the solid-phase is treated as discrete particles, and described by Newton's laws of motion on a single particle scale, discrete particle modeling, [4-6]. The advantage of the EL approach is that it allows studying the individual particle motion and particle-particle interactions directly, but this model requires powerful computational resources in large systems of particles, which is the case of FB. In the EE approach [7-11], both the gas- and solid-phases are considered as fluids and as fully interpenetrating continua. Both phases are described by separate conservation equations for mass and momentum. The EE approach is not limited by the particle number and becomes a more natural choice for hydrodynamic modeling of engineering scale systems [12, 13]. However, additional closure equations are required in the EE approach to describe the stochastic motion and interaction of the solid-phase. The kinetic theory of granular flow (KTGF) is commonly used to obtain constitutive relations for the solid-phase. The particles in gas-solid flow may be treated as magnified molecules, and the analogy of their behavior to the gas molecules is the reason for the wide use of the KTGF for modeling the motion of particles. This theory is basically an extension of the classical kinetic theory of non-uniform gasses [14] to dense particulate flows. The KTGF is based on the concept of granular temperature, what is the measure of random oscillations of the particles and is defined as the average of the three variances of the particle's velocities.

Within the framework of the EE approach, applying a proper drag model is very important, where it should be taken into account that, in spite of detailed mathematical modeling of the complex processes in FB, the drag laws used in two-fluid models are semi-empirical in nature. The interphase interaction drag force model [15] is often used. In that model, the coefficient between the fluid and solid (granular) phase depends only on the phase void fraction and the terminal velocity coefficient, not on the minimum fluidization conditions. Therefore, correction constants in the expression for the terminal velocity coefficient should be performed, which is particularly important in the case of fluidization with chemical reactions [16, 17].

In this paper, the EE approach, also called granular flow model (GFM), has been chosen to simulate the combustion of a liquid fuel in a 2-D BFB reactor. Within GFM calculation,

the third-phase has also been included in the process, which corresponds to a liquid fuel that is fed into the FB. The proposed numerical procedure also contains energy equations for all three phases, as well as the transport equations of chemical components with source terms due to the conversion of chemical species. The complex combustion model contains the homogeneous reactions of gaseous components, heterogeneous reactions with liquid fuel evaporation and direct combustion of liquid fuel.

The numerical simulation procedure is here applied to analyze the impacts of the different fluidization regimes on the efficiency of liquid fuels combustion in FB furnaces. For this purpose, the numerical experiments with liquid fuel, which chemical characteristics are similar to diesel fuel (chemical formula is $C_{10}H_{22}$), were conducted. The verification of the proposed numerical simulation procedure was based on a comparison of calculated temperature profiles along middle vertical distribution with experimentally obtained data. The experiments with the model fuel (sunflower oil) combustion in FB have been carried out on in-house BFB pilot facility.

Numerical simulation model of liquid fuels combustion in the FB reactor

The GFM approach of three-phase BFB comes down to the EE fluidization model that considers gas-particle interaction, taking into account the third-liquid-phase. The basic EE FB modeling approach considers the gas and FB dense phase, gas-particle system under conditions of the minimum fluidization [18], as two fluids with different characteristics. The transport equations for momentum transfer of the FB dense phase take into account fluid-particle interactions in conditions of the minimum fluidization velocity, as well as the interaction between the particles themselves. In this case, the third-liquid-phase has been included, because of the fuel fed into FB. The interaction between the liquid-phase and the gas as well as solid-phase have been separately modeled. In the EE approach, all phases have the same pressure and that is the pressure of the continuous primary phase. This model solves the continuity and momentum equations for each phase and tracks the volume fractions. Further, the additional transport equation for the granular temperature (which represents the solids fluctuating energy) is solved, and the solids bulk and shear viscosity are determined using the kinetic theory of gasses on granular flow. The basic EE fluidization model is upgraded here with a model of the liquid fuel devolatilization and homogenous and heterogeneous combustion.

Governing equations of the three-phase BFB model

For modeling the interactions between the gas, particle and liquid-phases, within the suggested EE granular approach to FB modeling, the routines incorporated in the modules of the commercial CFD software package FLUENT 14.0 were used. This code allows the presence of several phases within one control volume of the numerical grid, by introducing the volume fraction of each phase. The solid-phase represents a granular layer made of spherical particles, with uniform diameters. The mass and momentum conservation equations are solved for each phase separately.

The basic and constitutive equations of the EE granular model of the FB, taking into account the third-liquid-phase, can be described by the following set of expressions [19, 20]:

– continuity equation of the gas-phase

$$\frac{\partial}{\partial t}(\alpha_g \rho_g) + \nabla(\alpha_g \rho_g \vec{u}_g) = S_{ev} \tag{1}$$

– continuity equation of the solid-phase

$$\frac{\partial}{\partial t}(\alpha_s \rho_s) + \nabla(\alpha_s \rho_s \vec{u}_s) = 0 \tag{2}$$

– continuity equation of the liquid-phase

$$\frac{\partial}{\partial t}(\alpha_l \rho_l) + \nabla(\alpha_l \rho_l \vec{u}_l) = -S_{ev} \tag{3}$$

– momentum conservation equation of the gas-phase

$$\frac{\partial}{\partial t}(\alpha_g \rho_g \vec{u}_g) + \nabla(\alpha_g \rho_g \vec{u}_g \vec{u}_g) = -\alpha_g \nabla p + \nabla \bar{\bar{\tau}}_g + \alpha_g \rho_g \vec{g} + K_{gs}(\vec{u}_g - \vec{u}_s) + K_{gl}(\vec{u}_g - \vec{u}_l) \tag{4}$$

– momentum conservation equation of the solid-phase

$$\frac{\partial}{\partial t}(\alpha_s \rho_s \vec{u}_s) + \nabla(\alpha_s \rho_s \vec{u}_s \vec{u}_s) = -\alpha_s \nabla p - \nabla p_s + \nabla \bar{\bar{\tau}}_s + \alpha_s \rho_s \vec{g} + K_{gs}(\vec{u}_g - \vec{u}_s) + K_{ls}(\vec{u}_l - \vec{u}_s) \tag{5}$$

– momentum conservation equation of the liquid-phase

$$\frac{\partial}{\partial t}(\alpha_l \rho_l \vec{u}_l) + \nabla(\alpha_l \rho_l \vec{u}_l \vec{u}_l) = -\alpha_l \nabla p + \nabla \bar{\bar{\tau}}_l + \alpha_l \rho_l \vec{g} + K_{gl}(\vec{u}_g - \vec{u}_l) + K_{sl}(\vec{u}_s - \vec{u}_l) \tag{6}$$

were S_{ev} is the source and sink due to liquid fuel evaporation.

The stress tensors of the gas, granular liquid-phases can be expressed, respectively [17]:

$$\bar{\bar{\tau}}_g = 2\mu_g \bar{S}_g + (\lambda_g - \frac{2}{3}\mu_g)\nabla \vec{u}_g \bar{\bar{I}} \tag{7}$$

$$\bar{\bar{\tau}}_s = -p_s \bar{\bar{I}} + 2\alpha_s \mu_s \bar{S}_s + \alpha_s(\lambda_s - \frac{2}{3}\mu_s)\nabla \vec{u}_s \bar{\bar{I}} \tag{8}$$

$$\bar{\bar{\tau}}_l = 2\mu_l \bar{S}_l + (\lambda_l - \frac{2}{3}\mu_l)\nabla \vec{u}_l \bar{\bar{I}} \tag{9}$$

The last term of the eqs. (4) and (5) is a consequence of the inter-phase interaction drag force, where the coefficient between the fluid and solid (granular) phase, according to the Syamlal-O'Brien model [15], is:

$$K_{gs} = \frac{3\alpha_g \alpha_s \rho g}{4 u_{r,s}^2 d_s} C_D \left|\vec{u}_s - \vec{u}_g\right|, \qquad C_D = \left(0.63 + \frac{4.8}{\sqrt{\frac{\mathrm{Re}_s}{u_{r,s}}}}\right)^2, \qquad \mathrm{Re}_s = \frac{\rho_g d_s \left|\vec{u}_s - \vec{u}_g\right|}{\mu_g} \tag{10}$$

The terminal velocity coefficient for the solid-phase $u_{r,s}$ was determined:

$$u_{r,s} = 0.5\left[A - 0.06\,\mathrm{Re}_s + \sqrt{(0.06\,\mathrm{Re}_s)^2 + 0.12\,\mathrm{Re}_s(2B - A) + A^2}\right]$$
$$A = \alpha_g^{4.14}, \quad B = \begin{cases} = a\alpha_g^{1.28} & \text{for} \quad \alpha_g \le 0.85 \\ = \alpha_g^{b} & \text{for} \quad \alpha_g > 0.85 \end{cases} \tag{11}$$

The default values of the constants a and b in the coefficient B, eq. (11), are 0.8 and 2.65, respectively. However, despite the rigorous mathematical modeling of the associated physics, the drag laws used in the model continue to be semi-empirical in nature. The semi-empirical procedure is proposed primarily for prediction the drag law coefficients that correspond to real minimum fluidization conditions. The constants $a = 0.8$ and $b = 2.65$ in the coefficient B of the Syamlal-O'Brien interphase interaction drag force model, eqs. (10) and (11) are not universal, particularly when it comes to the fluidization regimes with multi-component fluid and in the non-isothermal conditions [16].

The momentum conservation eqs. (4) and (5) of the gas- and solid-phase have additional interphase drag force terms, due to the presence of liquid-phase. Both of these drag force terms: $K_{gl}(\vec{u}_g - \vec{u}_l)$ and $K_{sl}(\vec{u}_s - \vec{u}_l)$, respectively, also appear in the momentum conservation equations of the liquid-phase, eq. (6). For this case, the liquid-phase has secondary phase characteristics, same as the solid-phase. For fluid-fluid flows, each secondary phase is assumed to have a form of droplets or bubbles [20].

For the simulation of air-liquid interaction, the drag function model of Schiller and Naumann [20] has been used. Here, the interphase exchange coefficient between liquid and the solid-phase is obtained by Gidaspow *et al.* [21] drag model. It is a combination of Wen and Yu model and the Ergun equation in [20].

Equations for energy and conservation of chemical components

Section *Governing equations of the three-phase BFB model* shows the CFD model of a BFB that contains one more phase-liquid fuel, whilst in this chapter, it is described how the numerical procedure has been upgraded by introducing the devolatilization and combustion models.

The proposed combustion model includes the energy equations and the transport equations of chemical species conservation with the source terms due to the conversion of chemical components, which are presented:

– energy equation of gas-phase

$$\frac{\partial}{\partial t}(\alpha_g \rho_g c_{p,g} T_g) + \nabla(\alpha_g \rho_g \vec{u}_g c_{p,g} T_g) = \nabla\left(\frac{k_g}{c_{p,g}} \nabla T_g\right) +$$

$$+\nabla\left(\sum_i \alpha_g \rho_g D_{i,m} c_{p,i} T_g \nabla Y_i\right) + \sum R_i H_{r,l} - h_{sg}\left(T_s - T_g\right) - h_{gl}\left(T_g - T_l\right) \tag{12}$$

– energy equation of solid-phase

$$\frac{\partial}{\partial t}(\alpha_s \rho_s c_{p,s} T_s) + \nabla(\alpha_s \rho_s \vec{u}_s c_{p,s} T_s) = \nabla\left(\frac{k_s}{c_{p,s}} \nabla T_s\right) + h_{sg}\left(T_s - T_g\right) + h_{sl}\left(T_s - T_l\right) \tag{13}$$

– energy equation of liquid-phase

$$\frac{\partial}{\partial t}(\alpha_l \rho_l c_{p,l} T_l) + \nabla(\alpha_l \rho_l \vec{u}_l c_{p,l} T_l) = \nabla\left(\frac{k_l}{c_{p,l}} \nabla T_l\right) +$$

$$+\nabla\left(\sum_i \alpha_l \rho_l D_{i,m} c_{p,i} T_l \nabla Y_i\right) - h_{sl}\left(T_s - T_l\right) + h_{gl}\left(T_g - T_l\right) \tag{14}$$

– conservation equations for chemical components

$$\frac{\partial}{\partial t}(\alpha_k \rho_k Y_i) + \nabla(\alpha_k \rho_k \vec{u}_k Y_i) = \nabla(\alpha_k \rho_k D_{i,m} \nabla Y_i) + R_i \quad k = \text{g}, \text{l} \tag{15}$$

The energy balance equations for all three phases are connected through the interphase volumetric heat transfer coefficient, h, which has given by Gunn [22] for gas-solid and liquid-solid interphase heat transfer. For the gas-liquid interphase volumetric heat transfer coefficient, h_{gl}, the formulation of Ranz and Maeshall [23, 24] has been used. The granular conductivity coefficient, for conditions of the developed fluidization, has very high values (≈100 W/mK) [18]. The radiation heat transfer is not included in this stage of the model developing. This assumption may be valid if it is taken into account that the convective heat transfer and conduction in BFB are very intensive [18].

The source term R_i in a set of eq. (15) corresponds to the chemical conversion rates of the components i. The chemical reactions, used for combustion model within presented numerical procedure for liquid fuels combustion in FB, are homogeneous and heterogeneous. The homogeneous reactions are first step combustion of the evaporated fuel (to CO and H_2O) and CO oxidation, while heterogeneous reactions are liquid fuel evaporation and the first step of the direct liquid fuel combustion. The list of the numerical model reactions is shown in tab. 1.

Table 1. List of the numerical model reactions

Reaction description	Reaction formula	Reaction type
Fuel devolatilzation	$C_{10}H_{22(\text{liquid})} \rightarrow C_{10}H_{22(\text{gas})}$	Heterogeneous (modeled)
Liquid fuel first step oxidation	$C_{10}H_{22(\text{liquid})} + 10.5\ O_2 \rightarrow 10\ CO + 11\ H_2O$	Heterogeneous – finite rate: k_o = 2.59E12, E_a = 2.6E8
Evaporated fuel first step oxidation	$C_{10}H_{22(\text{gas})} + 10.5\ O_2 \rightarrow 10\ CO + 11\ H_2O$	Homogeneous – finite rate: k_o = 2.587E11, E_a = 1.256E8
CO oxidation	$CO + 0.5\ O_2 \rightarrow CO_2$	Homogeneous – finite rate: k_o = 1.0E12, E_a = 1.0E8

The production and conversion of species i due to the chemical reactions enter as a source/sink term R_i in the transport equations of chemical species:

$$R_i = M_i \sum_{l=1}^{N_R} (\nu''_{il} - \nu'_{il}) k_l \left(\prod_{j=1}^{N_l} C^{n'_{jl}} - \frac{1}{K_c} \prod_{j=1}^{N_l} C^{n''_{jl}} \right) \tag{16}$$

where N_R is the number of reactions l, N_l – the number of components j of reactants and products in reaction l, and n'_{jl}, n''_{jl} – the rate exponents for reactant and product species j in reaction l, respectively. The laminar finite rate reactions have been assumed for all homogeneous combustion processes and for the first step of the direct liquid fuel combustion, where the reaction rate constants k_l are determined by the Arrhenius expression:

$$k_l = k_{o,l} T^a \exp\left(-\frac{E_{a,l}}{\text{R}T} \right) \tag{17}$$

The reaction rate, R_i, for the fuel vaporization reaction (source terms in eqs. (1) and (3) – S_{ev}) has to be separately modeled. The mathematical modeling of the evaporation of the liquid fuel fed in fluidized furnace had to be differently considered if the temperature of the fuel is equal or lower than the boiling point of the fuel.

In the literature, an analysis of the prediction of the discrete phase droplet convective boiling can be found [25]. However, the here considered case, based on a continuous introduction of a liquid fuel into the hot FB, significantly differs from the discrete phase droplet convective boiling.

Generally, the global devolatilization rate of fuel is equal to the fuel flow. However, locally the devolatilization rate depends on the local fuel temperature and the contact surface with the FB. According to this, it is possible to evaluate the zone (*i. e.* surface) of non-evaporated fuel using balance equation:

$$\dot{m}_{\mathrm{fu}} c_{p,\mathrm{fu}} (T_{bp} - T_o) + \dot{m}_{vp} q_{\mathrm{lat}} = h_{fb} S_{\mathrm{l}} (T_{fb} - T_{bp}) \tag{18}$$

where $\dot{m}_{\mathrm{fu}}$ and $\dot{m}_{\mathrm{vp}}$ are the mass flows of fuel and vapor, respectively, T_o and $T_{fb} = (T_s + T_g)/2$ are temperatures of inlet fuel and FB temperature, respectively, q_{lat} – the fuel evaporation latent heat, h_{fb} – the convective heat transfer, and S_{l} – the heat transfer surface. Thus heat transfer surface is possible to evaluate when $\dot{m}_{\mathrm{vp}}$ is equal to $\dot{m}_{\mathrm{fu}}$.

Here, a simpler approach is used to calculate the local devolatilization rate. It depends only on the fuel temperature in the FB, whereby the effects of contact and mixing between the fuel and the FB are taken into account within the proposed numerical simulation of the FB with the added liquid-phase (fuel). In this case, the local source due to evaporated fuel can be determined using the following expression:

$$\dot{m}_{\mathrm{vp,l}} = \dot{m}_{\mathrm{fu}} \frac{T_{\mathrm{fu}} - T_o}{T_{bp} - T_o} Y_{\mathrm{fu}} \alpha_{\mathrm{s}} \tag{19}$$

where T_{fu} is the liquid fuel temperature which is $\leq T_{bp}$.

Numerical procedure

For solving the system transport equations of the proposed EE model for liquid fuel combustion in BFB the software package FLUENT 14.0 was used. For the models for the drag force and liquid fuel devolatilization, the particular subroutines have been in-house developed.

The calculations were non-stationary, with a time step of 1 ms, which allowed a relatively quick convergence with a maximum of 100 iterations per time step, whereby the convergence criterion between two iterations was set to $1 \cdot 10^{-3}$. The number of time steps, *i. e.* the total simulation time, has been determined by the time required for the fluid to pass through the entire reactor space. The computational domain consists of the two zones: a layer of particles in the FB and the free flow above the FB. The finite volume method is applied for the spatial discretization of the governing eqs. (1)-(6), and eqs. (12)-(15) and the variable arrangement is collocated. The solution domain was discretized by a structured non-orthogonal grid. The numerical grid consisted of 13130 nodes, where 3430 nodes used for granular bed zone.

The interphase interaction drag force model eqs. (10) and (11), [20, 21] as well as equations for the reaction rate constants for the fuel vaporization reactions, were included in the numerical simulation process by the specialized subroutines.

The interaction between the liquid-phase and the gas, as well as solid-phase, has been separately modeled. For the interphase interaction drag force definition, the model by Syamlal-O'Brien has been used, wherein the constants *a* and *b* of the model coefficient *B*, eq. (11), have values of 3.2 and 0.6625, respectively. For the simulation of air-liquid interaction, the drag function *f* model of Schiller and Naumann has been used. The interphase exchange coefficient between liquid and the solid-phase is obtained by Gidaspow drag model.

The proposed calculation procedure is performed through two steps: the calculation of transformation of the fixed granular bed to the fully developed bubble fluidization but without the fuel flow (section *Governing equations of the three-phase BFB model*) for desired hydrodynamic conditions and continuing the calculation procedure with the fuel flow introduction and including the combustion model (section *Equations for energy and conservation of chemical components*). The matrix values of the variables calculated in the first computing step were used as the initial conditions for the second step of the calculating process. Moreover, in the second step, the boundary conditions are changed introducing the inlet fuel flow and the equations of chemical species with the source terms due to chemical reactions were activated. The calculation process is ended when the quasi-stationary conditions are reached, *i. e.* when the mean values of calculated thermophysical properties are changed within the constant range.

All cases of numerical simulation of the processes in a fluidized combustion chamber were performed on the fluidization reactor with a height of 2.3 m and width of 0.4 m, as it is shown in the schematic view of the reactor [26]. The modeled granular bed consists of sand particles with the diameter of 0.8 mm and particle density of 2600 kg/m^3 (deposited density was 1310 kg/m^3) where the height of the bed in the bulk condition is 0.3 m. The fuel was entering through the vertical nozzle placed axially on the bottom of the reactor. The height of the nozzle for the fuel introduction is 0.05 m. Air for fluidization was introducing annularly. The inlet temperature of the air and fuel was ambient (300 K).

Figure 1 presents the solid volume fraction contours given by the proposed numerical procedure when is simulated the process of transition stagnant granular layer in the fluidized state. The simulated fluidization development, shown in fig. 1, was obtained for sand particles fluidized with air which ensures the fluidization number $N_f \approx 3$ on the temperature of 1200 K. The fluidization number is the ratio between of the fluidization gas velocity and the minimum fluidization velocity and represents a measure of the mixing intensity in FB. Numerical simulation of the bubbled fluidization development, fig. 1, presents the first step of the calculation procedure of the proposed combustion in FB numerical simulation.

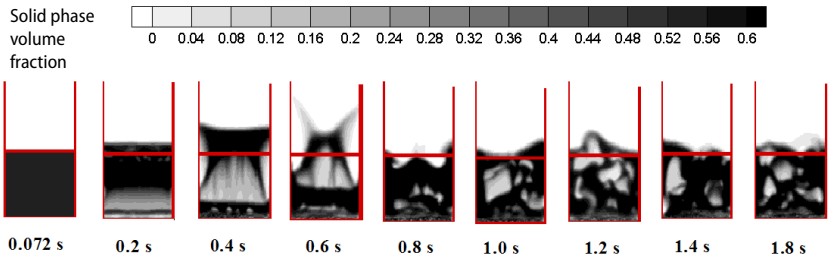

Figure 1. Simulation of the fluidization process from the stagnant layer within the fluidized reactor before the combustion is started

Experiments with combustion of the jet-fed fuel into the FB

The experiments with combustion in the fluidization furnace were done on a pilot facility, described elsewhere [26]. The experimental installation has been dimensioned, designed and built in a way that the results obtained during investigations on it can be used as design parameters for the construction of real-scale facilities for combustion of solid or liquid fuels. The furnace has a rectangular cross-section of 0.295 × 0.290 m and height of 2.3 m. The power of

the experimental chamber is up to 100 kW. The schematic view of the pilot facility is shown in fig. 2.

In the analyzed case, the fuel (sunflower oil) was fed into the FB at the angle of 38˚, and it was possible to regulate the distance of the nozzle outlet from the bed bottom.

The fuel is introduced into the experimental facility with the fuel feeding system through the tubular nozzle. The FB inert material consisted of quartz sand particles with a medium diameter of 0.8 mm, deposited density of 1310 kg/m^3 and the height of 0.323 m. The fluidization gas was air. The air is supplied to the FB through the distributor. The flue gasses from the particles burn out in the furnace space above the bed.

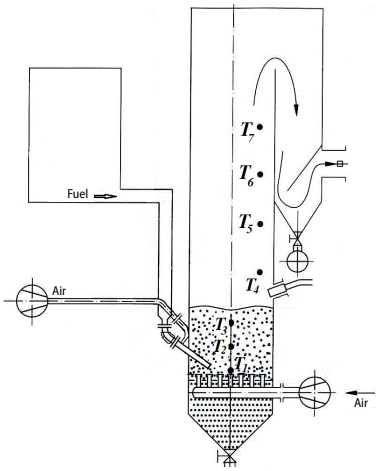

Figure 2. Schematic view of the pilot fluidized reactor

During the stationary regime of the furnace operation, temperatures inside the FB and concentrations of the combustion products were monitored continuously. The temperature measuring points along the vertical center line of the reactor are placed at the following distances from the nozzles (in mm): T_2 – 5, T_3 – 115, T_4 – 255, T_5 – 445, T_6 – 985, T_7 – 1415, and T_8 – 2385 (T_1 is the ambient temperature).

Experiments were conducted with the model fuel – sunflower oil, with and without adding water to the model fuel. The low heating value if the fuel was 37.1 MJ/kg. Volatile and char content in the fuel was 99.17 and 0.73 mas%, respectively, and humidity was 0.1 mas%.

The stationary regimes of combustion of model fuel were followed, tab. 2, for different immersing depths of the nozzle in the FB and for different compositions of the model fuel [26].

Table 2. Operating parameters of experimental FB furnace

Regime	Fuel flow rate [kgh^{-1}]	Air flow rate [kgh^{-1}]	Air fuel equivalence ratio	N_f	Temperature of the active part of the FB [°C]				Gas composition				Furnace power [kW]
					T_2	T_3	T_4	T_5	CO_2	O_2	CO	NO	
									[%]		[ppm]		
Model-fuel	4.08	142.7	2.95	3.34	663.3	898.3	899.2	904.9	5.1	14.95	16.18	12,18	42

In all the investigated regimes, stable combustion conditions were achieved, with the average bed temperature of 850-900 °C, which would get stabilized soon after the start. Very favorable emissions were achieved, with very low CO emissions.

Results of the numerical simulations and comparison with experimental results

The proposed numerical simulation procedure is applied to the analysis of the impacts on the different fluidization regime (different fluidization numbers) on the efficiency of liquid fuels combustion in furnaces with FB. Primarily the location and dimensions of the fuel com-

plete incineration area as a function of the fluidization number have been investigated. For this purpose, the calculations of test fuel combustion with three different fluidization numbers were carried out applying the procedure described in the section *Experiments with combustion of the jet-fed fuel into the FB*. The test fuels chemical formula is same as a diesel fuel ($C_{10}H_{22}$), but thermophysical and thermochemical properties correspond to sunflower oil, which is important because of the comparison with experiments were conducted with sunflower oil (section *Experiments with combustion of the jet-fed fuel into the FB*).

Table 3 contains the basic features of the liquid fuel combustion regimes which are simulated using the proposed procedure of the FB combustion chamber numerical modeling. Some of the parameters in tab. 3 are obtained by using the in-house made an iterative model of the ideal fuel temperature combustion [27].

Table 3. Basic features of the simulated combustion regimes

Regime	Fuel flow rate [kgh^{-1}]	Air flow rate [kgh^{-1}]	Air fuel equivalence ratio	N_f	Theoretical combustion temperature [°C]	Theoretical gas composition		Furnace power [kW]
						CO_2	O_2	
						Vol %		
1	7	314.8	3	2.37	936.3	4.63	14.36	91.4
2	9.31	418.6	3	3.15	936.5	4.63	14.36	121.5
3	12	539.6	3	4.06	936.3	4.63	14.36	156.7

As it can be seen in tab. 3, all three considered regimes have the same air-fuel equivalence ratio and therefore they have also the same theoretical combustion temperature and the theoretical combustion products gas composition. The main differences of the considered regimes are relating to the degree of stirring in the FB (fluidization number) and to the flows of fuel and air, and therefore to the power of the combustion chamber.

Figure 3 shows the results of the gas temperature distributions for given regimes, tab. 3, and at three different moments for each regime, obtained applying the proposed 2-D numerical simulation procedure of model fuel combustion in BFB. Gas temperature distributions shown in fig. 3 represent the thermal conditions within the fluidized reactor for the period starting from 4.7 to 6.7 seconds after the fuel introduction into the heated FB. The temperature field in the zone of intense reaction in fluidized combustion chamber stochastically changes in time but within a constant temperature range, so a quasi-stationary process can be assumed in that type of FB combustion.

At the first glance, it can be seen in fig. 3 that the zone of higher temperatures is located within FB in the case of Regime 2, while at the other two regimes the high temperatures appear in the freeboard. This leads to the conclusion that in these combustion conditions the Regime 2 ($N_f = 3.15$) is most favorable from the point of view of achieving the minimum zone of intensive reactions.

In order to get a clearer comparison of the considered combustion regimes temperature profiles the diagrams of averaged temperatures (at the time and in the reactor cross-section) along the reactor vertical axis are formed. Figure 4 shows the dimensionless temperature profiles along the central vertical line of the FB derived by proposed numerical model for considered three regimes, which are compared to experimental results presented in the section *Experiments with combustion of the jet-fed fuel into the FB*. It should be noted that the terms of the experiments closest match to the characteristics of the Regime 2.

The ordinate in the diagram of fig. 4 represents a dimensionless temperature: $\theta = (T - T_o)/(T_{max} - T_o)$, where T is given temperature, T_o – the ambient temperature, and T_{max} – the

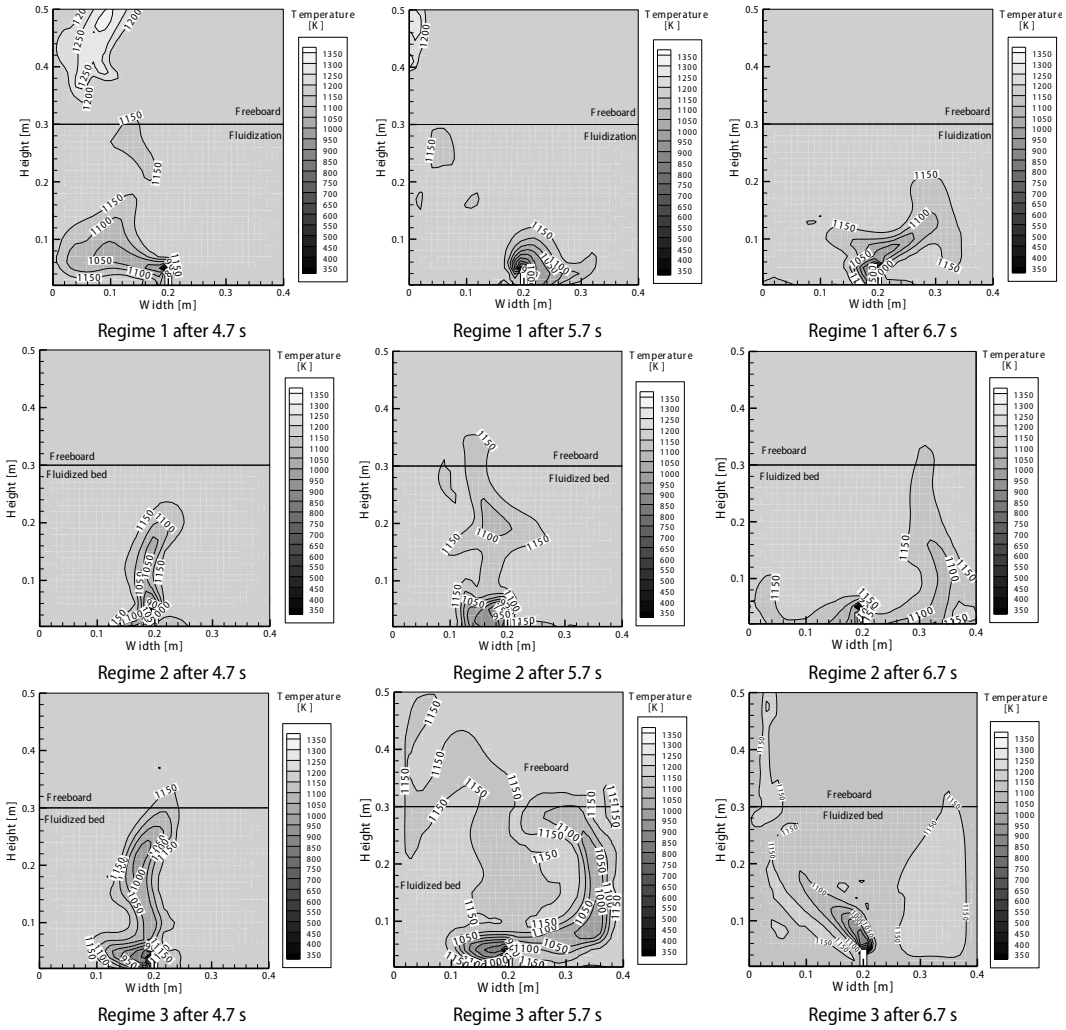

Figure 3. Calculated gas temperature distributions for model fuel combustion at three fluidization regimes and at three different moments for each regime

maximum temperature (theoretical combustion temperature) in the given conditions. Thereby, it should be noted that the axial temperature profile, obtained by the model, have been formed by averaging of the temperatures at the cross-sections at the considered heights of the reactor. Also on the presented diagrams, the abscissa represents the dimensionless height of the furnace, which is defined as the ratio between the height of the reactor and the height of the fixed bed (H/H_{mf}).

The dimensionless temperature profiles in fig. 4 obtained by the numerical simulation with combustion conditions corresponding to Regime 2 and profiles obtained from the experiments are in good agreement, what could be expected because the conditions of the experiments, tab. 2, were closest to the characteristics of the Regime 2, tab. 3. The deviations between the results obtained by experiment and model are observed only in the zone of freeboard because the experimental reactor was not ideally isolated in this area, while the model implies a fully adiabatic combustion.

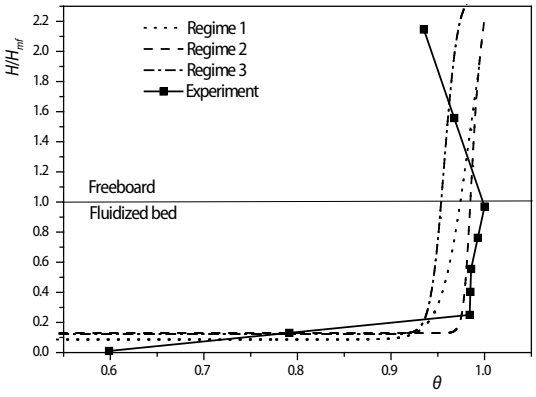

Figure 4. Normalized temperature profiles along fluidized combustor height numerically and experimentally obtained

The general conclusion that can be obtained on the basis of the diagram in fig. 4 is that temperature profiles along the central vertical line of the FB combustor obtained by measurements as well as by calculation show that very high temperatures can be achieved on relatively low heights of the reactor. In other words, both experiments and numerical simulations show that in considered FB combustor, the intense combustion zones have been withdrawn deep into the FB. This is very convenient because it provides efficient and complete combustion within a relatively small volume. Nevertheless, the influence of the fluidization number on the temperature profiles character along the height of the reactor is evident. The main differences of the considered regimes (Regime 1-3) are relating to fluidization number, N_f. As seen in fig. 4, the fuel combustion in FB at conditions of Regime 2 (and experiments), were fluidization number is 3.15, allows complete combustion in the lower zones of the reactor, while in the case of the combustion at lower and higher fluidization number, major part of the combustion process takes place above the bed. This leads to the conclusion that for considered combustion conditions the fluidization number which is 3.15 allows to some degree increased withdrawal of the intense combustion zone in FB furnace towards the lower zones. This also agrees with the analyses carried out on the basis of fig. 3. In the case of less than optimal fluidization numbers ($N_f = 3.15$) the reactants are not sufficiently mixed within FB, and the heterogeneous reactions have a lower rate (section *Equations for energy and conservation of chemical components*), so the intensive combustion zone moves towards higher areas of the reactor. On the other hand, at higher fluidization air flows (N_f is larger than optimal one) also comes to the withdrawal of intensive combustion zone toward the freeboard, due to combustion with high values of air-fuel equivalence ratio.

A similar conclusion can be drawn on the basis of fig. 5, which contains the profile diagrams of the averaged vaporized fuel mass fraction for all three regimes. As it can be seen in fig. 5 for Regime 2 ($N_f = 3.15$) the evaporated fuel conversion takes place mainly within the FB ($H/H_{mf} \approx 1$), while for two other regimes complete the fuel vapor combustion is performed in somewhat higher zones. This once again confirms that there is an optimal fluidization number for the combustion of liquid fuels in FB was the chemical process is fully carried out in the smallest volume. The furnace workpiece volume optimization could be of importance in the planning, design, and construction of industrial incinerators with FB.

The higher working space volume within complete combustion in the FB takes place for higher than optimal fluidization numbers is not a result of the lower rates of chemical reactions, but is the effect of a large air-fuel equivalence ratio and of the great value of Peclet number. On the other hand, in the case of less than optimal fluidization numbers ($N_f = 3.15$), the heterogeneous reactions have a lower rate, so the intensive combustion zone moves towards higher areas of the reactor. This is illustrated in fig. 6 which shows the averaged (by time and FB volume) liquid fuel evaporation rate for all three considered fluidization regimes (1.255E-04, 1.704E-04, and 1.971E-04 kgmol/m^{3}s^1 for regimes 1-3 from tab. 3). Only the heterogeneous reaction of liquid fuel evaporation is taken into consideration because it is the slowest reaction

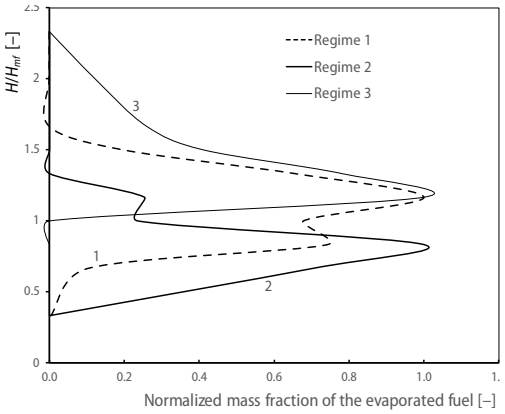

Figure 5. Calculated averaged evaporated fuel mass fractions along the reactor height

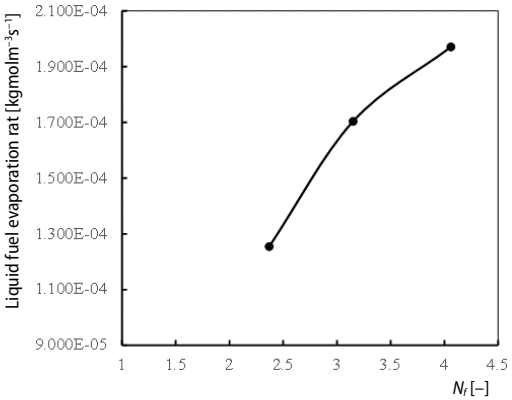

Figure 6. Liquid fuel evaporation rate in the function of the fluidization number

in the fluidization reactor and is a limiting factor in the entire chain of reactions. As seen from the table, the intensity of the reaction rate of fuel evaporation continually increases with fluidization number, which is contrary to the effect of the complete combustion zone volume dependence of N_f were this functional relation have a minimum.

Conclusions

A numerical CFD model of the liquid fuels combustion in a 2-D BFB has been proposed. The model is based on the EE granular flow simulation method including the KTGF for the particles motion modeling. The basic KTGF model is upgraded by the inclusion the liquid-phase due to fuel and also by the including evaporation and combustion models.

Because of the way of fuel dosing the processes in an experimental combustion chamber have a 3-D character. However, due to the complexity of the numerical simulation of FB with the chemical reactions here were applied the model equations in 2-D form, and fuel dosage is set symmetrically at 5 cm from the distribution plate. All other parameters: geometric, temperature, flow rates, chemical composition, *etc.*, correspond to the experimental conditions.

The developed numerical simulation procedure has been applied to the analysis of the different fluidization regime impacts on the efficiency of liquid fuels combustion in FB furnaces. For this purpose, the calculations of test fuel combustion with three different fluidization numbers were carried out. The results of temperature field calculation were compared with the experiments in-house provided on a BFB pilot facility. The general conclusion that can be obtained on the basis of the performed numerical simulations is that temperature profiles along the central vertical line of the FB combustor obtained by measurements as well as by calculation show that very high temperatures can be achieved on relatively low heights of the reactor. This leads to the conclusion that efficient and complete combustion is accomplished within a relatively small volume, what could be of importance for the FB incinerators design. The dimensionless temperature profiles along the reactor central vertical line obtained by numerical simulation with combustion conditions corresponding to Regime 2 and profiles obtained from the experiments are in good agreement.

Analyzing the calculated dimensionless temperature profiles, as well as diagrams of the averaged vaporized fuel mass fraction for all three simulated regimes, it can be concluded that there is an optimal fluidization regime from the point of view of the zone size in which

combustion is completely accomplished. For considered combustion conditions the fluidization number which is 3.15 leads to some degree increased indentation of the intense combustion zone in FB furnace towards the lower reactor zones. The intensity of the reaction rate of fuel evaporation continually increases with fluidization number, which is contrary to the effect of the complete combustion zone volume dependence of N_f were this functional relation have a minimum.

Acknowledgment

The authors wish to thank the Serbian Ministry of Education, Science and Technological Development for financing the project *Improvement of the industrial fluidized bed facility, in the scope of technology for energy efficient and environmentally feasible combustion of various waste materials in fluidized bed*, Project TR33042.

Nomenclature

C – molar concentration, [kmol·m^{-3}]
C_D – drag coefficient, [–]
c_p – specific heat, [Jkg^{-1}K^{-1}]
$D_{i,m}$ – mass diffusion coefficient for species i, [m^{2}s^{-1}]
d_s – particle mean diameter, [m]
E_a – Activation energy, [Jmol^{-3}]
$\vec{g}$ – gravity acceleration, [ms^{-2}]
H – height, [m]
H_{mf} – height of the fixed bed, [m]
H_{rl} – heating value of reaction l, [Jkg^{-1}]
h – heat transfer coefficient with specific surface, [Wm^{-2}K^{-1}]
h_{fb} – heat transfer coefficient between fuel and FB, [Wm^{-2}K^{-1}]
$\bar{\bar{I}}$ – unity matrix, [–]
K_c – reaction equilibrium constant, [–]
K_{gl} – gas/liquid momentum exchange, [kg·s^{-1}]
K_{gs} – gas/solid momentum exchange, [kg·s^{-1}]
K_{sl} – solid/liquid momentum exchange, [kg·s^{-1}]
k – thermal conductivity, [Wm^{-1}K^{-1}]
k_o – pre-exponential coefficient, [s^{-1}]
M_i – molar mass of species i, [kgmol^{-1}]
N_f – fluidization number, [–]
p – pressure, [Pa]
$\underline{R}$ – universal gas constant, [Jmol^{-1}K^{-1}]
$\bar{\bar{S}}_k$ – strain rate tensor, (k = s, g, l), [–]
T – absolute temperature, [K]
T_{bp} – temperature of the boiling point, [K]
T_{max} – maximal temperature in the regime, [K]
$\vec{u}$ – instantaneous velocity vector, [m·s^{-1}]
Y_{fu} – fuel mass fraction, [–]
Y_i – component i mass fraction, [–]

Greek symbols

α – phase void fraction, [–]
λ – bulk viscosity, [kgm^{-1}s^{-1}]
μ – kinetic viscosity, [kgm^{-1}s^{-1}]
ν – stoichiometric number, mole number, [–]
ρ – density, [kgm^{-3}]
$\bar{\bar{\tau}}$ – phase stress-strain tensor, [Pa]

Subscripts

ev – evaporator
fb – fluidized bed
fu – fuel
g – gas
l – liquid, number of reaction
s – solid

Superscripts

“ – products
‘ – reactants

References

[1] Saxena, S., Jotshi, C., Fluidized-Bed Incineration of Waste Materials, *Progress in Energy and Combustion Science*, *20* (1994), 4, pp. 281-324
[2] Tsuji, Y., *et al.*, Discrete Particle Simulation of Two-Dimensional Fluidized Bed, *Powder Technology*, *77* (1993), 1, pp. 79-87
[3] Hoomans, B., *et al.*, Discrete Particle Simulation of Bubble and Slug Formation in a Two-Dimensional Gas-Fluidised Bed: A Hard-Sphere Approach, *Chemical Engineering Science*, *51* (1996), 1, pp. 99-118
[4] Gera, D., *et al.*, Computer Simulation of Bubbles in Large-Particle Fluidized Beds, *Powder Technology*, *98* (1998), 1, pp. 38-47
[5] Ibsen, C. H., *et al.*, Comparison of Multifluid and Discrete Particle Modelling in Numerical Predictions of Gas Particle Flow in Circulating Fluidised Beds, *Powder Technology*, *149* (2004), 1, pp. 29-41

[6] Bokkers, G., *et al.*, Mixing and Segregation in a Bidisperse Gas-Solid Fluidised Bed: A Numerical and Experimental Study, *Powder Technology*, *140* (2004), 3, pp. 176-186
[7] Di Renzo, A., Di Maio, F. P., Homogeneous and Bubbling Fluidization Regimes in Dem-CFD Simulations: Hydrodynamic Stability of Gas and Liquid Fluidized Beds, *Chemical Engineering Science*, *62* (2007), 1, pp. 116-130
[8] Enwald, H., *et al.*, Simulation of the Fluid Dynamics of a Bubbling Fluidized Bed, Experimental Validation of the Two-Fluid Model and Evaluation of a Parallel Multiblock Solver, *Chemical Engineering Science*, *54* (1999), 3, pp. 311-328
[9] Cammarata, L., *et al.*, 2D and 3D CFD Simulations of Bubbling Fluidized Beds Using Eulerian-Eulerian Models, *International Journal of Chemical Reactor Engineering*, *1* (2003), 1
[10] Behjat, Y., *et al.*, CFD Modeling of Hydrodynamic and Heat Transfer in Fluidized Bed Reactors, *International Communications in Heat and Mass Transfer*, *35* (2008), 3, pp. 357-368
[11] Gidaspow, D., *Multiphase Flow and Fluidization: Continuum and Kinetic Theory Descriptions,* Academic press, New York, USA, 1994
[12] Van Wachem, B., *et al.*, Comparative Analysis of CFD Models of Dense Gas-Solid Systems, *AIChE Journal*, *47* (2001), 5, pp. 1035-1051
[13] Van der Hoef, M. A., *et al.*, Computational Fluid Dynamics for Dense Gas-Solid Fluidized Beds: A Multi-Scale Modeling Strategy, *Chemical Engineering Science*, *59* (2004), 22, pp. 5157-5165
[14] Chapman, S., Cowling, T. G., *The Mathematical Theory of Non-Uniform Gases: An Account of the Kinetic Theory of Viscosity, Thermal Conduction and Diffusion in Gases,* Cambridge University Press, Cambridge, UK, 1970
[15] Syamlal, M., O'brien, T., Simulation of Granular Layer Inversion in Liquid Fluidized Beds, *International Journal of Multiphase Flow*, *14* (1988), 4, pp. 473-481
[16] Nemoda, S. Dj., *et al.*, Euler-Euler Granular Flow Model of Liquid Fuels Combustion in a Fluidized Reactor, *Journal of the Serbian Chemical Society*, *80* (2015), 3, pp. 377-389
[17] Nemoda, S. Dj., *et al.*, Three Phase Eulerian-Granular Model Applied on Numerical Simulation of Non-Conventional Liquid Fuels Combustion in a Bubbling Fluidized Bed, *Thermal Science*, *20*. (2016), Suppl. 1, pp. S133-S149
[18] Oka, S., *Fluidized Bed Combustion*, Marcel Dekker, Inc., New York, Basel, USA, 2004
[19] Vejahati, F., *et al.*, CFD Simulation of Gas-Solid Bubbling Fluidized Bed: A New Method for Adjusting Drag Law, *The Canadian Journal of Chemical Engineering*, *87* (2009), 1, pp. 19-30
[20] Pandey, S. K., Simulation of Hydrodynamics of Three Phase Fluidized Bed, M. Sc. thesis, National Institute of Technology, Orissa, India, 2009
[21] Gidaspow, D., *et al.*, Hydrodynamics of Circulating Fluidized Beds: Kinetic Theory Approach, Report Dept. of Chemical Engineering, Illinois Inst. of Tech., Chicago, Ill., USA, 1991
[22] Gunn, D., Transfer of Heat or Mass to Particles in Fixed and Fluidised Beds, *International Journal of Heat and Mass Transfer*, *21* (1978), 4, pp. 467-476
[23] Ranz, W., Marshall, W., Evaporation from Drops, Part I, *Chem. Eng. Prog*, *48* (1952), 3, pp. 141-146
[24] Ranz, W., Marshall, W., Evaporation from Drops, Part II, *Chem. Eng. Prog*, *48* (1952), 4, pp. 173-180
[25] Kuo, K. K., *Principles of Combustion,* John Wilea and Sons Inc., New York, USA, 1996
[26] Mladenović, M. R., *et al.,* Vertical Temperature Profile in the Installation for the Combustion of Waste Fuels in the Fluidized Bed Furnace, *Proceedings*, Conference on CD-ROM, 15th Symposium on Thermal Science and Engineering of Serbia, Soko Banja, Serbia pp. 18-21
[27] Nemoda, S. Dj., *et al.*, Numerical Calculation and Measurement of the Coal Powder Distribution in Burner's Channels with Louvers and Analysis of Related Theoretical Combustion Temperatures on TPP Nikola Tesla-A6 Boilers, *Termotehnika*, *37* (2011), 2, pp. 223-240

Paper submitted: September 22, 2017
Paper revised: October 10, 2017
Paper accepted: December 18, 2017